Int. J. Electrochem. Sci., 17 **(2022)** Article Number: 220836, doi: 10.20964/2022.08.31

International Journal of
ELECTROCHEMICAL
SCIENCE
www.electrochemsci.org

Research on SOC Estimation for Lithium ion batteries Based on Improved PNGV Equivalence Model and AF-UKF Algorithm

Heng Zhou[1], *Shunli Wang*[1,*], *Chunmei Yu*[1], *Lili Xia*[1], *Carlos Fernandez*[2]

[1] School of Information Engineering, Southwest University of Science and Technology, Mianyang 621010, China;
[2] School of Pharmacy and Life Sciences, Robert Gordon University, Aberdeen AB10-7GJ, UK.
[*]E-mail: 497420789@qq.com

Received: 1 May 2022 / *Accepted:* 8 June 2022 / *Published:* 4 July 2022

Accurately estimating the state of charge of lithium-ion batteries is of great significance for real-time monitoring and safety control of batteries. To solve the problems of difficult real-time estimation and low estimation accuracy of lithium batteries under various operating conditions, the ternary lithium-ion battery is used as the research object to establish an improved partnership for a new generation of vehicles(PNGV) equivalent circuit model to characterize the operating characteristics of the battery and to study and analyze the operating characteristics of the lithium battery by comprehensive experiments under various operating conditions. Considering the importance of state of charge accuracy at the early stage of estimation for the later estimation, the initial value of estimation is firstly calibrated using the open-circuit voltage method, and then the adaptive fading unscented Kalman filter algorithm is used for estimation tracking to achieve high accuracy estimation of lithium battery state of charge in real-time. A simulation model is built in MATLAB/Simulink and the performance analysis is carried out with a variety of operating conditions. The experimental results show that the improved PNGV model can better estimate the state of charge of lithium batteries with fast convergence, good tracking effect, and a maximum error of 0.485%. Comparing the state of charge results estimated using the adaptive fading unscented Kalman filter (AF-UKF) algorithm with the unscented Kalman filter algorithm, the maximum error was reduced by 0.354% in the HPPC condition and 1.978% in the BBDST condition, improving the accuracy and convergence speed of the filter.

Keywords: Lithium-ion battery; Improve PNGV model; State of charge; Adaptive Fading Unscented Kalman filtering algorithm;

1. INTRODUCTION

With the advancement of technology and social development, the global energy crisis and environmental pollution problems are becoming more and more serious, which has caused widespread

concern in the world[1]. As a result, countries around the world are committed to researching and developing new energy sources[2] to alleviate the energy crisis and environmental pollution problems[3]. Lithium batteries have been widely used and developed in the field of new energy[4] because of their high energy density, low discharge rate, long life, high output power, and green environmental protection[5]. The State of Charge (SOC) of lithium batteries is an indicator describing the remaining power of the battery[6] and is one of the most important parameters in the process of battery use[7]. Accurate SOC estimation is a key factor limiting the rapid development of new energy vehicles[8].

The common methods for estimating the SOC of lithium batteries are divided into two categories[9]: one is the direct measurement for estimation, including the ampere-time integration method[10] and the open-circuit voltage method[11]; the other is the intelligent estimation method based on the battery model, including the neural network method and the Kalman filter algorithm[12]. Among them, the open-circuit voltage method battery rebound characteristics require the battery to sit for a long time to get the accurate open-circuit voltage[13], which can not meet the real-time SOC estimation[14]; the ampere-time integration method meets the real-time problem, but the initial value of SOC is difficult to determine[15], as well as the error increases with the accumulation of time, making it difficult to achieve accurate SOC estimation[16]; the neural network method relies on the accuracy of training data[17], which requires a large amount of data and calculation. The algorithm is complex and difficult to use online[18]; the Kalman filter algorithm, although it can obtain accurate values even when the initial value of SOC is inaccurate and the computation is small, is suitable for online estimation of SOC[19], but it needs to rely on an accurate battery model[20]. At present, the mainstream method for estimating the SOC of lithium batteries is the Kalman filter algorithm[21, 22]. To improve the accuracy of the traditional Kalman filter algorithm for estimating SOC, many scholars have conducted a lot of research to optimize the Kalman filter algorithm[23].

This research is aim to accurately describe the operating state of ternary lithium batteries[22], consider the accuracy of characterization and computational complexity, develop an improved PNGV equivalent circuit model for lithium batteries[24], use the Adaptive Fading Unscented Kalman Filter (AF-UKF) algorithm to estimate the SOC of lithium batteries[25], and compare the estimation effect of the Unscented Kalman Filter (UKF) algorithm[26].

2. BATTERY STATE-SPACE MODEL

2.1 Equivalent circuit model

The battery model can visually characterize the relationship between the external characteristics of the battery (voltage, current, temperature, etc.) and the internal state quantities (SOC, resistance, electric potential, etc.), and establish mathematical expressions for the relationship, thus enabling the internal state quantities to be calculated indirectly based on the external characteristics of the battery[27]. Among the many equivalent circuit models, the Thevenin model[28] only considers the rapid changes in polarization response of the battery. The Rint model[29] does not consider the polarization

characteristics of battery, so its accuracy is not ideal. The second-order RC[29] equivalent circuit model considers the slow change process of the battery polarization reaction, has a small amount of calculation and high accuracy, but it is more suitable for online parameter identification. The PNGV model takes into account the influence of the battery state and operating conditions on the model parameters, and can more accurately describe the characteristics of the battery[30]. The improved PNGV model add a parallel RC link in the PNGV model, and the two RC links correspond to the two poles in the impedance spectrum of lithium batteries, which more accurately describes the polarization phenomenon of lithium batteries. It has higher accuracy and practicality than other models, so it is chosen in this paper.

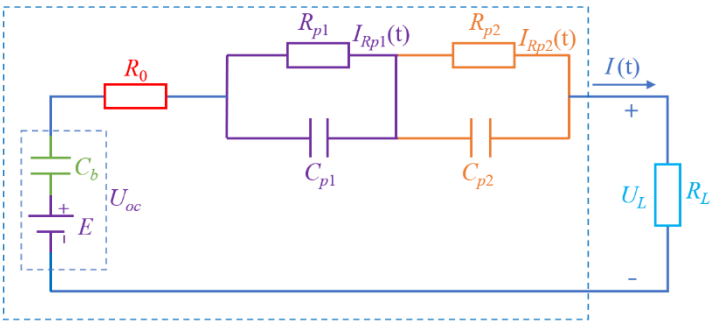

Figure 1. Lithium-ion battery improved PNGV equivalent circuit model

The improved PNGV model is shown in Figure 1, E is the ideal voltage source, representing the open-circuit voltage of the battery; capacitance C_b describes the change in open-circuit voltage generated by the accumulation of current; E and C_b together represent the change in open circuit voltage U_{OC}; R_0 is the ohmic internal resistance of the battery; R_{p1} and R_{p2} are the two polarized internal resistances of the battery; C_{p1} and C_{p2} are the two polarized capacitors of the battery, composed of RC and series links together simulates the polarization characteristics of the battery; I is the current of the battery loop; U_L is the terminal voltage of the battery. Under constant temperature experimental conditions and neglecting the effect of current, the component parameters of the model are a function of the SOC of the battery. The relationship between the battery terminal voltage and current is established based on the circuit model, as shown in equation (1).

$$U_L = U_{OC} - R_0 I_L - I_{p1} R_{p1} - I_{p2} R_{p2} \tag{1}$$

Using the knowledge of modern control theory, the equivalent circuit model can be discretized and the mathematical model established is shown in equations (2) and (3). Equation (2) for the k moment and k+1 moment battery SOC value S_k and polarization voltage U_{p1}, U_{p2} recurrence relationship, equation (3) for the k moment battery terminal voltage U_k and current i_k and SOC value S_k relationship.

$$\begin{pmatrix} S_{k+1} \\ U_{k+1}^{p1} \\ U_{k+1}^{p2} \end{pmatrix} = \begin{pmatrix} 1 & 0 & 0 \\ 0 & exp(-\Delta t/\tau_1) & 0 \\ 0 & 0 & exp(-\Delta t/\tau_2) \end{pmatrix} \begin{pmatrix} S_k \\ U_k^{p1} \\ U_k^{p2} \end{pmatrix} + \begin{pmatrix} -\dfrac{\Delta t}{Q} \\ R_{p1}(1 - exp(-\Delta t/\tau_1)) \\ R_{p2}(1 - exp(-\Delta t/\tau_2)) \end{pmatrix} i_k \tag{2}$$

$$U_k = U_{OCV}(S_k) - i_k R_0 - U_k^{p1} - U_k^{p2} \tag{3}$$

Here Δt is the sampling time interval, τ_1 and τ_2 are the time constants for each of the two RC parallel links, $\tau_1 = R_{p1}C_{p1}$, $\tau_2 = R_{p2}C_{p2}$ and Q is the battery capacity.

2.2 Parameter identification

This paper selected a 4.2V/72Ah ternary lithium battery as the object of study. To obtain the voltage and current data required for the model parameter identification, HPPC tests were conducted on the ternary lithium battery to analyze the working process of the battery under specific temperature conditions to obtain the required parameters. The pulse test was carried out at an interval of 0.1 for SOC and the parameters were identified according to the experimental voltage curve. The pulse test voltage curve at SOC=0.7 is shown in Fig. 2.

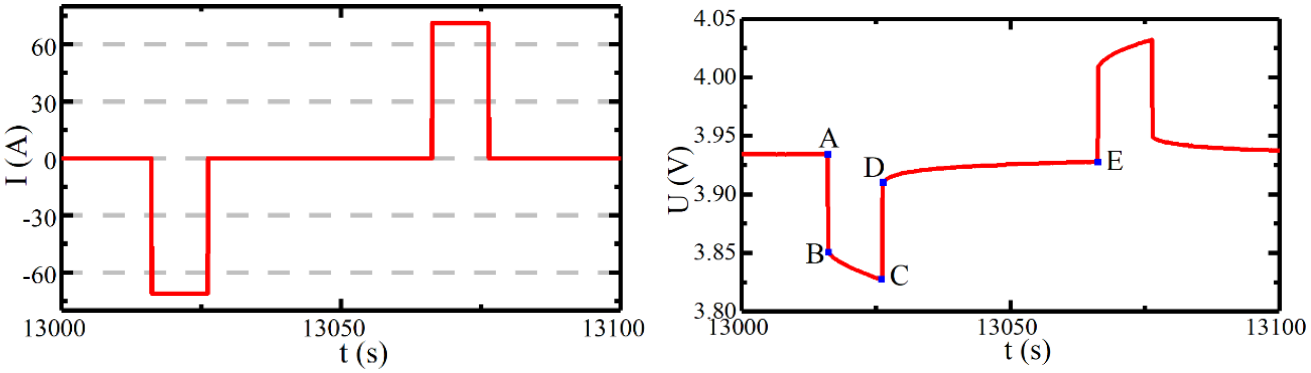

(a) Pulse test current curve (b) Pulse test voltage curve

Figure 2. Pulse test current and voltage curve at SOC = 0.7

Analysis of Figure 2 (b) shows that the vertical drop in voltage at the moment of discharge is due to the transient voltage drop caused by the presence of the battery ohmic internal resistance R_0, I is the discharge current, from which the battery ohmic internal resistance can be obtained as shown in equation (4).

$$R_0 = \frac{|U_A - U_B|}{I} \tag{4}$$

The identification process and results for C_b are shown in equations (5) and (6).

$$\Delta Q U_{OCV} = \frac{1}{2} C_b [(U_{OCV} + \Delta U_{OCV})^2 - U^2{}_{OCV}] \tag{5}$$

$$C_b = \frac{\Delta Q}{\Delta U_{OCV}} \tag{6}$$

According to the conservation of energy, equation (5) is simplified to obtain equation (6), where is the discharge power, obtained from experimental data, and is the voltage difference caused by the integration of the discharge current across the polarization capacitor, i.e.,$U_A - U_E$.

The identification of the polarization resistor and polarization capacitor is relatively complex. At the end of the discharge, the voltage at the battery terminal rises slowly, which is the process of

discharging the polarization capacitor to the polarization resistor, and the mathematical expression for the zero-input response of the dual RC parallel link is shown in equation (7).

$$U_P = U_{P1} + U_{P2} = U_1 \exp\left(-\frac{t}{\tau_1}\right) + U_2 \exp\left(-\frac{t}{\tau_2}\right) \tag{7}$$

In equation (7), U_P is the sum of the series voltages, U_1 and U_2 are the initial polarization voltages respectively, τ_1 and τ_2 are obtained by curve fitting the target equation (7) using the experimental data.

When discharging, the voltage at the battery terminal slowly drops, which is the process of charging the polarization capacitor by the discharge current, and the mathematical expression for the zero-state response of its RC parallel circuit is shown in equation (8).

$$U_L = U_B - \frac{1}{C_b}\int Idt - IR_{P1}(1 - exp(-t/\tau_1)) - IR_{P2}(1 - exp(-t/\tau_2)) \tag{8}$$

By substituting τ_1 and τ_2 into equation (8) and curve fitting R_{p1} and R_{p2} as parameters to be determined, the polarization resistance parameters are obtained, and then the polarization capacitance C_{p1} and C_{p2} can be obtained from the time constant calculation equation $\tau_1 = R_{p_1}C_{p_1}$ and $\tau_1 = R_{p_2}C_{p_2}$.

3. ADAPTIVE FADING UNSCENTED KALMAN FILTER ALGORITHM

The UKF algorithm is essentially a high-precision transformation of a non-linear model through a linear interpolation method. Its disadvantages are that the covariance update is prone to negative definite matrices when the degree of non-linearity is strong and that the system noise is more pronounced due to the influence of the initial values. The unknown statistical properties of the noise in the data acquisition process can lead to a reduction in the estimation accuracy of the Kalman filter method, and can even cause divergence, resulting in unstable filtering results generating large errors. Therefore, a time-varying fading factor is introduced to attenuate the influence of past data on the current filter value, improve the robustness and accuracy of the filter, adaptively adjust the process noise and measurement noise covariance, improve the accuracy and convergence speed of the filter, and form an adaptive fading unscented Kalman filtering algorithm.

3.1 Introduction to the UKF algorithm

Following Kalman's recursive formula, an estimate of the state at the current moment is derived from the new data and the estimate of the previous state, with the aid of the system's state transfer equation. The discrete state-space equation for a non-linear system of lithium batteries is shown in equation (9).

$$\begin{cases} x_{k+1} = f(x_k, u_k) + w_k \\ y_k = g(x_k, u_k) + v_k \end{cases} \tag{9}$$

In Equation (9), f is the nonlinear state equation; g is the nonlinear observation equation; w_k, v_k are the Gaussian white noise of the random variable x and the observation variable y, whose variance matrices are Q_w and R_v, respectively, and whose expressions are shown in Equation (10).

$$\begin{cases} Q_w = E[w_k w_k^T] \\ R_v = E[v_k v_k^T] \end{cases} \tag{10}$$

The initialization $X_0 = (SOC_0, 0,0)$ is set to the initial value of the state variable with the expression for the variance estimate P_0 shown in equation (11).

$$P_0 = \begin{pmatrix} P_{SOC_0} & 0 & 0 \\ 0 & P_{S_0} & 0 \\ 0 & 0 & P_{P_0} \end{pmatrix} \tag{11}$$

The dimension of the state variable L=3 according to the statistic x_{k-1} of the state variable and its covariance P_{k-1}^x; the steps of the algorithm for estimating the lithium battery SOC based on the unscented Kalman filter of the UT transform are as follows.

(1) Calculating sampling points

Using the Sigma point symmetric sampling strategy, the set of Sigma points for point x is obtained, along with its corresponding weighted values w_i^m for the mean and variance, as shown in equation (12).

$$\begin{cases} X_0 = x_{k-1} \\ X_i = x_{k-1} + \left(\sqrt{(L+r)P_{k-1}^x}\right), i = 1,2,\dots,L \\ w_0^m = \dfrac{r}{L+r} \\ w_0^c = \dfrac{r}{L+r} + (1-\alpha^2+\beta) \\ w_0^m = w_0^c = \dfrac{1}{2(L+r)}, i = 1,2,\dots,L \end{cases} \tag{12}$$

In Equation (12), α and β are constants; the adaptive adjustment factor, $r = \alpha^2(L+\varepsilon) - L$, serves to adjust the higher-order matrix and reduce the prediction error; $0 \le \alpha \le 1$ is used to set the distance of these point sets to the mean point; ε is the second scale adjustment factor, usually set to 0; $\beta \ge 0$ is applied to incorporate the random variable x, which is optimal for a Gaussian prior distribution, β=2; and $(\sqrt{(L+r)P_{k-1}^x})_i$ denotes the ith column of the square root matrix of the weighted covariance matrix.

(2) Time Updates

The state update is calculated according to the state equation to obtain equation (13).

$$X_{k|k-1} = f(X_{k-1}, i_k) + q_k \tag{13}$$

Calculate the predicted state values as shown in equation (14).

$$x_k^- = \sum_{i=0}^{2L} (w_i^m X_{i,k|k-1}) \tag{14}$$

The covariance of the calculated state prediction values is shown in equation (15).

$$p_k^{x-} = \sum_{i=0}^{2L} w_i^c \left(X_{i,k|k-1} - x_k^-\right)\left(X_{i,k|k-1} - x_k^-\right)' + Q_k \tag{15}$$

Calculating the measurement update from the equation of state gives equation (16).

$$Y_{k|k-1} = g\left(X_{k|k-1}, i_k\right) + r_k \tag{16}$$

Calculate the predicted measurements as shown in equation (17).

$$y_k^- = \sum_{i=0}^{2L} (w_i^m Y_{i,k|k-1}) \tag{17}$$

The covariance of the calculated measurement estimate y_k^- is shown in equation (18).

$$p_k^{y-} = \sum_{i=0}^{2L} w_i^c \left(Y_{i,k|k-1} - y_k^-\right) \left(Y_{i,k|k-1} - y_k^-\right)' + R_k \tag{18}$$

The covariance between $X_{k|k-1}$ and $Y_{k|k-1}$ is calculated as shown in equation (19).

$$p_k^{xy} = \sum_{i=0}^{2L} w_i^c \left(X_{i,k|k-1} - x_k^-\right) \left(Y_{i,k|k-1} - y_k^-\right) \tag{19}$$

(3) Measurement updates

Calculate the Kalman gain matrix as shown in equation (20).

$$K_k = P_k^{xy} (P_k^{y-})^{-1} \tag{20}$$

Updating the state gives equation (21).

$$x_k = x_k^- + K_k (y_k - y_k^-) \tag{21}$$

Updating the error covariance yields equation (22).

$$P_k^x = P_k^{(x-)} - K_k \left(P_k^{(y-)}\right) K_k^T \tag{22}$$

3.2 AF-UKF algorithm

In order to effectively improve the accuracy of battery SOC estimation when the degree of non-linearity is strong, reduce the influence of initial values and system noise on the filtering results, and improve the stability of algorithm filtering. Based on the traditional UKF algorithm, an fading factor and an adaptive adjustment factor are introduced to form an adaptive unscented Kalman filter with an fading memory effect. As the system noise also affects the filtering results, the introduction of the adaptive adjustment factor adjusts the associated covariance matrix, which can change its role in the filtering process to a certain extent.

3.2.1 Fading factor

A fading factor is introduced on top of the UKF algorithm to form an unscented Kalman filter with a fading memory effect. The main difference between this algorithm and the traditional UKF algorithm is the addition of the fading factor S to equation (15), allowing equation (15) to be converted to equation (23).

$$p_k^{x-} = S \sum_{i=0}^{2L} w_i^c \left(X_{i,k|k-1} - x_k^-\right) \left(X_{i,k|k-1} - x_k^-\right)' + Q_k z \tag{23}$$

The selection of the fading factor S has a significant impact on the filtering results. The filtering accuracy decreases as S increases and sometimes even causes filtering divergence. Therefore, to effectively improve the filtering effect and system stability, it is also necessary to introduce an adaptive adjustment factor.

3.2.2 Adaptive adjustment factor

The traditional UKF algorithm is heavily influenced by the initial values and, in addition, system noise can also affect the filtering results. Therefore, to reduce these effects, adaptive adjustment of the associated covariance matrix can modify its role in the filtering process to some extent. Define $er_k = y_k - y_k^-$ and construct the adaptive factor $\alpha_k (0 \le \alpha_k \le 1)$ as shown in equation (24).

$$\alpha_k = \begin{cases} 1, tr(er_k er_k^T) \le tr(p_y^-) \\ \dfrac{tr(p_y^-)}{tr(er_k er_k^T)}, tr(er_k er_k^T) > tr(p_y^-) \end{cases} \tag{24}$$

The covariance matrix equation (18), (19) and (22) are modified to obtain equation (25).

$$\begin{cases} p_k^{y-} = \dfrac{1}{\alpha_k} \sum_{i=0}^{2L} w_i^c \left(Y_{i,k|k-1} - y_k^-\right) (Y_{i,k|k-1} - y_k^-)' + R_k \\ p_k^{xy} = \dfrac{1}{\alpha_k} \sum_{i=0}^{2L} w_i^c \left(X_{i,k|k-1} - x_k^-\right) \left(Y_{i,k|k-1} - y_k^-\right) \\ P_k^x = \dfrac{1}{\alpha_k} P_k^{(x-)} - K_k \left(P_k^{(y-)}\right) K_k^T \end{cases} \tag{25}$$

When there is an error in the initial value of the UKF algorithm or an abnormal disturbance in the system, the adaptive factor $\alpha_k < 1$, when the model prediction information makes a small contribution to the final filtered solution; when the prediction information is abnormal, $tr(er_k er_k^T)$ will be large, when the adaptive factor α_k is close to 0, and the prediction does not work at all.

4. ANALYSIS OF EXPERIMENTAL RESULTS

4.1 Test platform construction

In order to verify the accuracy of the battery model and algorithm, an experimental platform is to be set up to experimentally test the battery under different complex operating conditions. A lithium-ion aluminum-cased battery with a nominal capacity of 72Ah is used as the experimental object, and the entire battery test platform is shown in Figure 3. BTS200-100-104 is used to test the battery, TT-5166TH is used to provide a constant experience temperature to the battery, and the host computer is used to record the experimental data.

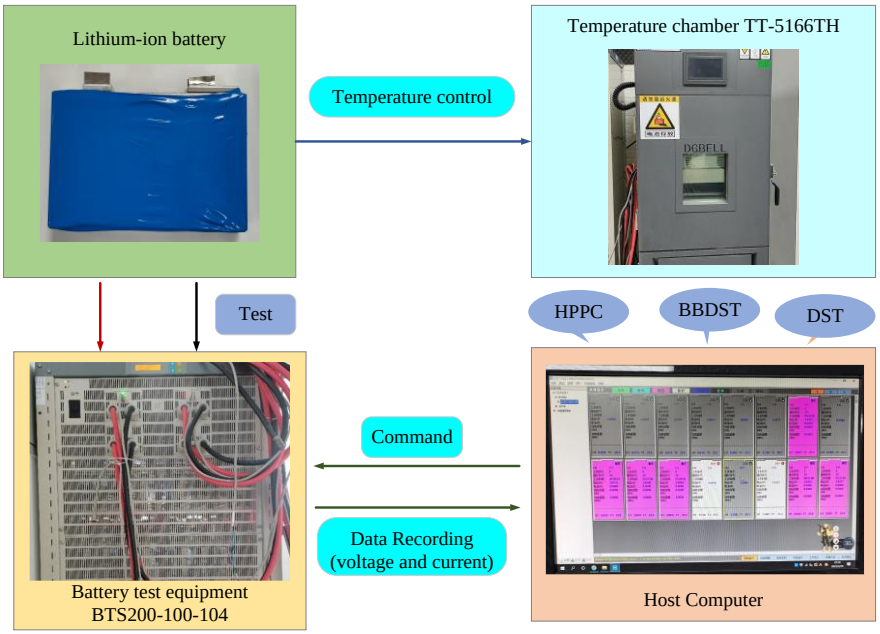

Figure 3. The entire battery test platform

4.2. Parameter identification results

For the parameter identification of the equivalent model, the lithium-ion battery was subjected to a pulse discharge test based on the theoretical basis of parameter identification in the previous section. The ohmic internal resistance R_0, capacitance C_b, polarization internal resistance R_{p1} and R_{p2}, polarization capacitance C_{p1} and C_{p2} and open-circuit voltage U_{oc} for the different SOC stages were calculated as shown in Table 1.

Table 1. Model parameters under different SOC states

SOC	R_0/Ω	R_{P1}/Ω	C_{P1}/F	R_{P2}/Ω	C_{P2}/F	C_b/F	U_{OC}/V
1	0.001152402	0.000484852	29309.13824	3.21689E-05	28863.44728	109967.9	4.1865
0.9	0.001172078	0.000538397	26230.28136	4.2934E-05	15173.65135	127839.0542	4.0504
0.8	0.001172078	0.000636351	26030.4755	4.71782E-05	16469.47697	221130.0215	3.9341
0.7	0.001183321	0.000609087	24073.34356	3.62726E-05	21862.8414	97720.49467	3.8306
0.6	0.001213536	0.000602201	23454.46934	3.8479E-05	18457.53059	80643.12667	3.731
0.5	0.001247967	0.000400249	31880.11385	3.32089E-05	23397.39068	154095.1465	3.6492
0.4	0.001264129	0.000404044	33600.06611	2.77279E-05	31010.08063	164951.85	3.6142
0.3	0.001297971	0.000504571	33534.35233	3.80466E-05	18936.25663	157766.2826	3.5859
0.2	0.001331587	0.000541348	27599.58755	4.97219E-05	12593.51462	126633.0254	3.5292
0.1	0.001494167	0.000736401	15103.50035	0.000145762	2276.208296	103207.8859	3.4495

The battery is basically in a stable state after each discharge and the voltage at this point is the Open Circuit Voltage (OCV) value corresponding to the current SOC. As can be seen from Table 1, the internal parameters of the improved PNGV model fluctuate within a certain range as the SOC changes, and if a more accurate simulation is required, the relationship between each parameter and the SOC needs to be obtained.

According to the values of R_0, R_{p1}, R_{p2}, C_{p1}, C_{p2}, C_b and U_{oc} model parameters derived from Table 1, the curve was fitted with the corresponding SOC values respectively, and the fitting order was set to 5th order to obtain the relationship curve between each model parameter and SOC, and the curve expression is shown in equation (26).

$$f(x) = p_1x^5 + p_2x^4 + p_3x^3 + p_4x^2 + p_5x^1 + p_6 \quad (26)$$

In Equation (26), x is the SOC and $f(x)$ is the parameter curve to be fitted, the results are shown in Table 2.

Table 2. Curve fitting results for each parameter

	R_0/Ω	R_{P1}/Ω	C_{P1}/F	R_{P2}/Ω	C_{P2}/F	C_b/F	U_{OC}/V
p_1	0.0465	-1.4644E7	9.7594E-6	-0.01184	-2.3178E6	-1.4016E7	4.41795
p_2	0.1717	3.7061E7	0.00125	0.03504	6.3963E6	3.3897E7	-15.01241
p_3	0.2391	-3.314E7	-0.0041	-0.04035	-6.2486E6	-2.8358E7	19.25601
p_4	0.1432	1.2201E7	0.0043	0.02266	2.4718E6	9.4182E6	-10.68227
p_5	0.0429	-1.4904E6	-0.0017	-0.00614	-287751.7832	-970421.2416	2.96627
p_6	0.0448	116405.206	3.596E-4	6.98809E-4	11664.2656	128258.5783	3.23984

After the model parameters were obtained, the accuracy of the model parameters was verified. The determined parameters were placed into the modified PNGV model with the same current input as the HPPC test experiment, the model output voltage response data was compared to the actual voltage data and the model estimation error was calculated. The voltage comparisons and error distributions are shown in Figure 4.

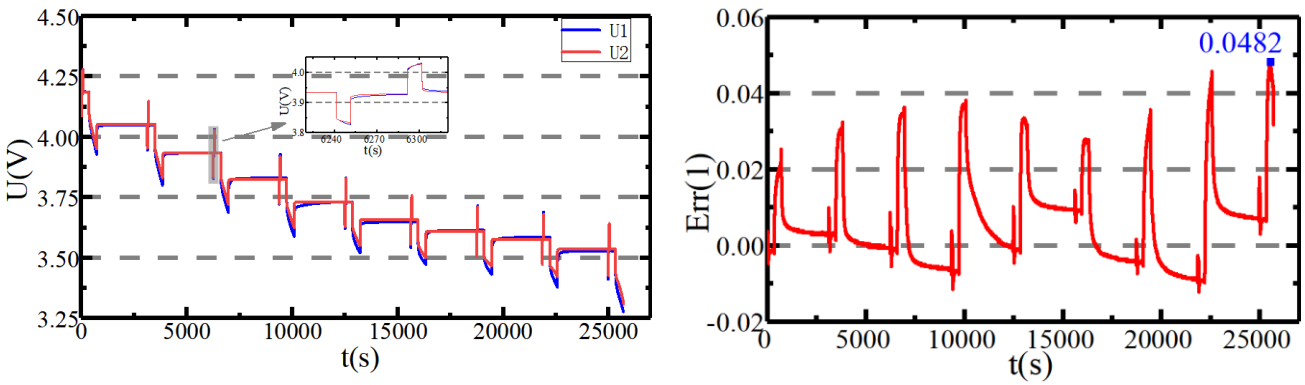

(a) Output voltage comparison curve (b) Error distribution curve

Figure 4. Output voltage comparison and error distribution curves

Based on the improved 2RC-PNGV, Y Y Liu[31] obtained that the maximum error in the output voltage is 0.11 V, and based on the PNGV model, W Li[32] obtained that the maximum error in the output voltage is 0.0922 V. From Figure 4 (b), it can be seen that the maximum error in the output voltage of the improved PNGV model is 0.0482V, indicating that the improved PNGV model has a good tracking effect and can represent the terminal voltage of the battery in operation.

4.3 HPPC working condition experiments

To verify the feasibility of the AF-UKF algorithm for Li-ion battery SOC estimation, a Li-ion battery SOC estimation model is constructed. The estimation accuracy of the model, the convergence of the estimation process, and the traceability to real data are investigated under a variety of experimental conditions.

Considering that batteries are often discharged intermittently in actual use, the model was further simulated and analyzed under HPPC experimental conditions, and the results were obtained by comparing the AF-UKF algorithm with the UKF algorithm as shown in Figure 5.

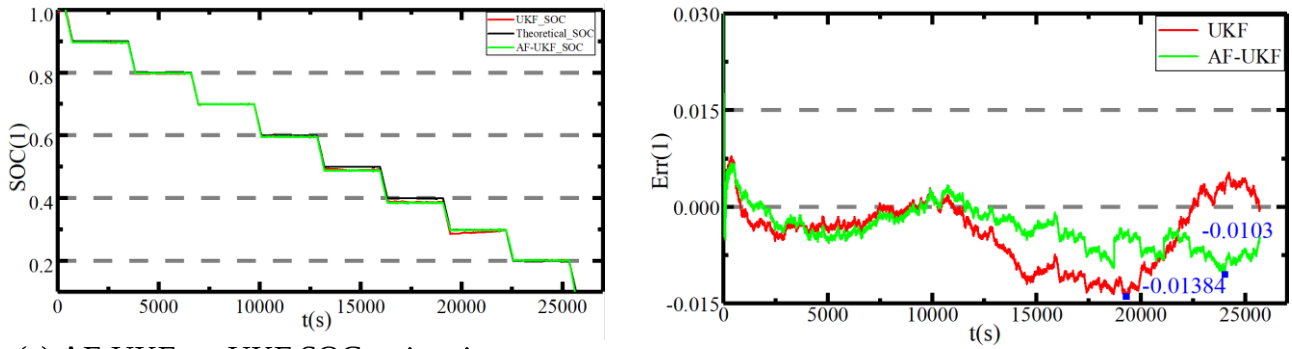

(a) AF-UKF vs. UKF SOC estimation curves

(b) Estimation error variation curve

Figure 5. Comparison of SOC estimation results under HPPC condition

In Figure 5(a), the theoretically calculated value and estimated values of the battery SOC using AF-UKF and UKF are shown respectively. Between 10,000 and 15,000s, the estimation error of UKF fluctuates considerably compared to AF-UKF, while AF-UKF is flatter around the theoretical estimate and the estimate is closer to the theoretical estimate, because AF-UKF has a stronger adaptive capability to changes in the noise model through real-time updating of the noise covariance and has better estimation performance. From Figure 5(b), it can be seen that the SOC estimation error of UKF is 1.384% and that of AF-UKF is 1.03%, a reduction of 0.354%, demonstrating better convergence and tracking of SOC estimation using AF-UKF.

4.4 BBDST working condition experiments

To further validate the response of the estimation algorithm to the Li-ion battery state of charge under more complex application conditions, the model is simulated and validated with experimental data

from the BBDST operating conditions. The UKF algorithm, under the same operating conditions, is also simulated and analyzed simultaneously to compare and highlight the advantages and disadvantages of the AF-UKF algorithm. The experimentally obtained voltage and current data were imported into the MATLAB workbench to analyze the estimated models. The results of comparing the battery SOC values with the theoretical values using UKF and AF-UKF, respectively, and the estimation errors are shown in Figure 6.

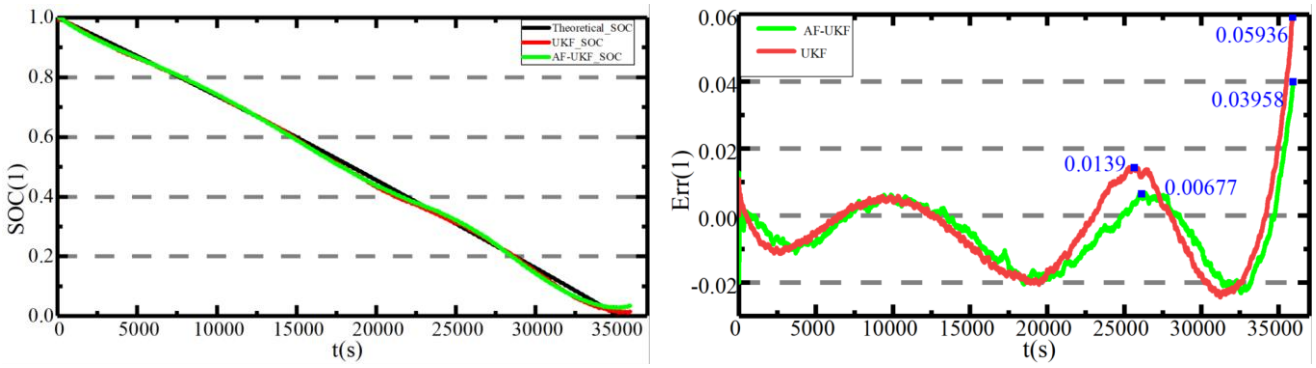

(a) AF-UKF vs. UKF SOC estimation curves (b) Estimation error variation curve

Figure 6. Comparison of SOC estimation results under BBDST condition

The convergence, as well as the tracking effect of the AF-UKF algorithm, can be seen in Fig. 6(a) to be comparable to UKF, but AF-UKF has higher accuracy. As can be seen from Figure 6(b), the maximum SOC estimation error is 5.936% for UKF and 3.958% for AF-UKF, which demonstrates the better convergence and tracking of SOC estimation using AF-UKF under BBDST conditions.

5. CONCLUSION

Accurate SOC estimation of Li-ion electrons is the focus and difficulty of Li-ion battery state monitoring. This paper characterizes the state and output characteristics of Li-ion batteries based on the improved PNGV model, conducts HPPC experiments for parameter identification, and determines the relationship between circuit model parameters and Li-ion battery charge state changes at different discharge stages. The Simulink model is built on MATLAB and simulated with experimental data under various operating conditions. The results show that the established estimation model can better estimate the SOC of Li-ion battery with a maximum estimation error of 0.482%, and the errors of AF-UKF under HPPC and BBDST operating conditions are 1.03% and 0.01% respectively, which are reduced by 0.354% and 0.0012% compared with the errors of UKF under HPPC and BBDST operating conditions respectively, verifying that the adaptive fading unscented Kalman has high accuracy in SOC estimation for Li-ion batteries.

References

1. Y. M. Feng, L. Tao, Z. F. Zheng, H. B. Huang and F. Lin, *Energy Storage Materials*, 31 (2020) 274.

2. X. F. Li and G. L. Cui, *Journal of Energy Storage*, 18 (2018) 285.
3. H. H. Zhang, Z. G. Zou, S. C. Zhang, J. Liu and S. L. Zhong, *International Journal of Electrochemical Science*, 15 (2020) 12041.
4. H. Y. Xiang, N. P. Deng, H. J. Zhao, X. X. Wang, L. Y. Wei, M. Wang, B. W. Cheng and W. M. Kang, *Journal of Energy Chemistry*, 58 (2021) 523.
5. H. P. Shan, H. Cao, X. Xu, T. Xiao, G. Y. Hou, H. Z. Cao, Y. P. Tang and G. Q. Zheng, *Journal of Solid State Electrochemistry*, 26 (2022) 163.
6. G. Z. Dong, J. W. Wei and Z. H. Chen, *Journal of Power Sources*, 328 (2016) 615.
7. J. J. Liu, Z. R. Wang, J. H. Gong, K. Liu, H. Wang and L. S. Guo, *Materials*, 10 (2017) 230.
8. T. T. Nguyen, A. B. Khan, Y. Ko and W. Choi, *Energies*, 13 (2020) 4536.
9. Z. Liu, W. Tang, X. Wang and P. Li, *China Mechanical Engineering*, 29 (2018) 1834.
10. W. K. Ji, S. L. Wang, C. A. Y. Zou and H. T. Shi, *International Journal of Electrochemical Science*, 16 (2021) 210737.
11. Y. J. Chen, G. Yang, X. Liu and Z. C. He, *Energies*, 12 (2019) 1803.
12. Y. Rong, W. Yang, H. Niu and X. Zheng, *Advanced Technology of Electrical Engineering and Energy*, 34 (2015) 22.
13. B. Ning, B. G. Cao, B. Wang and Z. Y. Zou, *Energy*, 153 (2018) 732.
14. C. Zhang, K. Li, L. Pei and C. B. Zhu, *Journal of Power Sources*, 283 (2015) 24.
15. B. Z. Xia, H. Q. Wang, Y. Tian, M. W. Wang, W. Sun and Z. H. Xu, *Energies*, 8 (2015) 5916.
16. Q. Wang, H. R. Gu, M. Ye, M. Wei and X. X. Xu, *Ieee Access*, 9 (2021) 83364.
17. Y. Zhang, H. Wu and C. Ye, *Energy Storage Science and Technology*, 10 (2021) 237.
18. C. Lin, A. H. Tang and J. L. Xing, *Applied Energy*, 207 (2017) 394.
19. D. D. Ge, Z. D. Zhang, X. D. Kong and Z. P. Wan, *Applied Sciences-Basel*, 11 (2021) 11797.
20. Y. D. Xu, M. H. Hu, C. Y. Fu, K. B. Cao, Z. Su and Z. Yang, *Electronics*, 8 (2019) 1012.
21. L. Y. Zhang, L. Zhang, C. Papavassiliou and S. Liu, *Wireless Personal Communications*, 102 (2018) 2063.
22. J. Wang, W. Yu, Y. Zhu and Z. Yin, *Ship Engineering*, 42 (2020) 15.
23. R. L. Du, J. Q. Liu, D. Zhou and G. Meng, *Proceedings of the Institution of Mechanical Engineers Part G-Journal of Aerospace Engineering*, 232 (2018) 3078.
24. L. Deng, X. Li, H. Wu, C. Yao and X. Wang, *Chinese Journal of Power Sources*, 41 (2017) 1461.
25. B. H. Du, Z. Yu, S. H. Yi, Y. L. He and Y. L. Luo, *International Journal of Low-Carbon Technologies*, 16 (2021) 927.
26. Z. Q. Wu, G. Y. Wang, Z. K. Xie, Y. L. He and X. Q. Lu, *Journal of Renewable and Sustainable Energy*, 12 (2020) 065501.
27. M. Chang, Y. Hou, X. Zhi, X. Zhao and G. Liang, *Chinese Journal of Power Sources*, 42 (2018) 1307.
28. H. W. He, R. Xiong, X. W. Zhang, F. C. Sun and J. X. Fan, *Ieee Transactions on Vehicular Technology*, 60 (2011) 1461.
29. Y. J. Zheng, W. K. Gao, M. G. Ouyang, L. G. Lu, L. Zhou and X. B. Han, *Journal of Power Sources*, 383 (2018) 50.
30. Y. Yang, T. Tang, D. Qin and M. Hu, *Journal of System Simulation*, 24 (2012) 938.
31. Y. Liu, S. Wang, Y. Xie, W. Ji and Y. Zhang, *Energy Storage Science and Technology*, 10 (2021) 2312.
32. W. Li, W. Liu and Y. Deng, *China Mechanical Engineering*, 31 (2020) 321